Chemistry Europe
European Chemical Societies Publishing

WILEY VCH

Excellence in Chemistry Research

Announcing our new flagship journal

- Gold Open Access
- Publishing charges waived
- Preprints welcome
- Edited by active scientists

Meet the Editors of *ChemistryEurope*

Luisa De Cola
Università degli Studi di Milano Statale, Italy

Ive Hermans
University of Wisconsin-Madison, USA

Ken Tanaka
Tokyo Institute of Technology, Japan

EurJIC
European Journal of Inorganic Chemistry

Research Article
doi.org/10.1002/ejic.202300343

Chemistry Europe
European Chemical Societies Publishing

www.eurjic.org

Accessibility of Lithium Cations in VSH-2 Zeotype: Structural Effects and Formation of Protonated Water Clusters

Rosa Micaela Danisi*[a] and Michael Fischer*[b, c]

The accessibility of lithium cations in microporous vanadosilicate VSH-2Cs of composition $Cs_2(VO)(Si_6O_{14})\cdot 3H_2O$ was investigated by Single Crystal X-ray Diffraction, Attenuated Total Reflection Fourier Transformed Infrared Spectroscopy and Density Functional Theory calculations. The topological symmetry of VSH-2Cs is described in space group *Cmca*. After Li-ion exchange, the structure of VSH-2Li adopted monoclinic symmetry (space group *C2/c*) with $a = 17.011(2)$ Å, $b = 8.8533(11)$ Å, $c = 12.4934(16)$ Å, $\beta = 91.677(4)°$, $V = 1880.7(4)$ Å^3. The strong interactions between Li ions and oxygen-framework atoms drive the main deformation mechanism, which is based on cooperative rotation of SiO_4 and VO_5 units around their oxygen atoms that behave as hinges. Exchange of Cs^+ by Li^+ is incomplete and accompanied by the formation of protonated species to counterbalance the electrostatic charge. The incorporation of protons is mediated by the presence of water dimers in the structural channels. H_2O molecules in VSH-2Li account not only as "space-fillers" after the removal of large Cs ions but also mediate proton transfer to compensate the negative charge of the host vanadosilicate framework.

Introduction

Zeotype materials containing metal cations (such as titanium, vanadium, zirconium, niobium, etc) possess not only classical zeolitic properties but also enable new technological applications.[1–3] For example, vanadium can exist in different coordination geometries and oxidation states, which allows for a number of heterogeneous catalyzed reactions.[4,5] The incorporation and stabilization of vanadium in porous framework creates functional materials with accessible active sites for acid-catalyzed and oxidation reactions.[6–8] However, the catalytic and adsorptive properties of such compounds depend not only on the structural properties dictated by the framework but also on the identity, quantity, location and coordination environment of extra-framework cations. The negatively charged surface of the framework provides a polar environment which can be modified by varying the number and type of charge compensating cations via conventional ion-exchange. Larger monovalent cations are generally preferred by frameworks with lower charge density and can locally balance the anionic charge of the host framework without appreciably distorting it.[9] Li^+, however, represents an exception because of the small ionic radius and concentrated charge. It can interact very strongly with sorbed molecules and significantly distort its host framework. The effect of Li^+ on porous structures has been already examined for some zeotype materials (in particular RHO topology[10]) but it remains substantially unexplored for a large variety of frameworks.

Precise knowledge of the cation distribution over available crystallographic sites is necessary to interpret the sorption and catalytic data obtained for developing specific properties. However, the coordination environment and accessibility of these extra-framework species are not always easy to determine. Cation distribution in zeotypes can be successfully characterized by X-ray diffraction methods.[11–13] Despite the great progress achieved by previous studies, there is still a lack of data on distribution of Li^+ ions in zeotype frameworks. The location of Li in complex porous structures in rather difficult to obtain due to the negligible X-ray scattering power of the Li atom.

We have been interested in the synthesis and structural characterization of zeotype vanadosilicate compounds (VSH-*n*A, where *n* is the framework type and A represents the extraframework cations) containing silicate tetrahedral sheets linked by square pyramidal $V^{4+}O_5$ units.[14,15] The pentahedral coordination of vanadium is characterized by four unequal equatorial distances V–O and one short apical vanadyl-type V=O bond of ca. 1.6 Å. The vanadium centers are accessible to molecular and cation species via the porous network with free channel

[a] *Dr. R. M. Danisi*
Technical Petrophysics, Institute of Applied Geosciences
Karlsruhe Institute of Technology
76131 Karlsruhe (Germany)
E-mail: rosamicaela.danisi@gmail.com

[b] *Dr. M. Fischer*
Crystallography and Geomaterials Research, Faculty of Geosciences
University of Bremen
28359 Bremen (Germany)
E-mail: michael.fischer@uni-bremen.de

[c] *Dr. M. Fischer*
MAPEX Center for Materials and Processes
and Bremen Center for Computational Materials Science
University of Bremen
28334 Bremen (Germany)

Supporting information for this article is available on the WWW under https://doi.org/10.1002/ejic.202300343

Research Article
doi.org/10.1002/ejic.202300343

diameters up to 6.5 Å.[15] The anionic nature of vanadosilicate framework results in the presence of charge-balancing cations and water molecules in the porous network. All VSH structures show excellent thermal stabilities up to 773 K and reversible dehydration-rehydration properties as confirmed by thermogravimetric analysis.[15]

Preliminary studies showed successful exchange of larger alkali cations by Li^+ in VSH frameworks.[15] Enhanced water adsorption capabilities were observed after Li ion-exchange of VSH-4Rb. The removal of large Rb cations increases the micropore volume and consequently the Li-exchanged sample contains one additional H_2O molecule per formula unit (pfu) compared to untreated VSH-4Rb.[15] However, the complete exchange of Li^+ in vanadosilicate frameworks remains elusive. In Li-exchanged VSH-12Cs, one of the three Li extraframework positions appears to be strongly underbonded with Li–O distances too long for the coordination requirement of Li cations, suggesting an incomplete exchange reaction. Similarly in VSH-16Na, only 2/3 of the Na^+ ions could be substituted by Li^+, leading to the formation of an alkali deficient framework.[16] Differences in the position and bond energy of the cationic sites seems to strongly affect the extent and kinetics of the cation exchange in VSH-16Na. The exclusion of small Li^+ cations at specific exchange sites is compensated by the presence of larger hydronium H_3O^+ species, interacting with their environment exclusively through hydrogen bonds, to maintain the framework electroneutrality.[16]

To further investigate Li^+ exchange and interactions with VSH frameworks, we selected VSH-2Cs of composition $Cs_2(VO)Si_6O_{14}\cdot 3H_2O$, which is a prospective material for size-selective adsorption of molecules and ion-exchange.[17] This material is a small-pore zeotype, whose channels have a width defined by 8-membered rings (8MR) and a free aperture of 3.0×3.6 Å. The polyhedral framework has a negative charge of $2e^-$ pfu, which is compensated by the incorporation of Cs cations into the channel system. The total surface area, obtained from N_2 adsorption, of VSH-2Cs is 40 m^2/g, indicating that a significant portion of the pores is blocked by the large Cs^+ cations.[17] The surface area increased to 149 m^2/g upon exchanging Cs^+ with Na^+.[17] The exchange with Li would increase not only the surface area but also the performance of VSH-2Li in gas separation and storage application.

The nature of the electronic transitions in VSH-2Cs was investigated using UV/Vis spectroscopy. The absorption bands in the 200–400 nm region were attributed to the charge-transfer (CT) interaction among the V^{4+}, O^{2-}, and M^{n+} countercation. Moreover, it was shown that λ_{max} of the UV-region absorption band and the band-gap E_g are progressively red-shifted with increasing electronegativity of the counter cation in the dehydrated state. This reveals the occurrence of V^{4+}-to-framework O^{2-} charge transfer or metal-to-ligand charge transfer (MLCT) and, simultaneously, a ligand-to-metal charge-transfer (LMCT) between O^{2-} and M^{n+} countercation. This phenomenon was shown also in vanadosilicates AM-6[18] and VSH-1 K.[19]

Our investigation is aiming to explore the influence of Li substitution on the host VSH-2 structure. Understanding the structural changes induced by the Li ion-exchange in vanadosilicate frameworks is indeed of great interest since the physicochemical properties of these materials are potentially enhanced.[20] Exchange of larger Cs^+ by small Li^+ cations may lead to incomplete reactions due to steric effects or by the inability of the negative charge distribution of the host framework to accommodate the Li^+ cations. In this regard, VSH-2Cs has a low framework charge density and is potentially prone to experience strong distortions from the electric fields at the surface of highly polarizing cations such as Li^+. We use Single-Crystal X-ray diffraction (SC-XRD) to characterize the structure before and after the ion-exchange, Attenuated Total Reflection Fourier Transformed Infrared Spectroscopy (ATR-FTIR) and Density Functional Theory (DFT) calculations to gain information of the coordination environment of the adsorbed H_2O molecules in the porous channels. A key open question, which we will address in the discussion part, is whether the adsorbed water during the ion-exchange process acts as merely "space-filler" or plays a fundamental role in charge balancing the host framework after Li^+ ion-exchange.

Results and Discussion

Lithium ion-exchange and phase transformation

The VSH-2Cs material crystallizes as distorted octahedral crystals (Figure 1). Single-crystal X-ray diffraction data collection, refinement parameters, atomic coordinates and displacement parameters are given in Tables 1–5. The structure of VSH-2Cs is characterized by silicate layers bridged by VO_5 square-based pyramids. The silicate layer is composed of single tetrahedral chains running along [001]. The orientation of the tetrahedra in the chains is *UUQDD*, where a four-connected *Q* tetrahedron with no terminal corner is inserted between apical pairs pointing up and down along **a** (Figure 2). The tetrahedral chains are laterally joined to form 4- and 6- membered rings, as visualized in Figure 2 and the connection of adjacent silicate layers by VO_5 pyramids is that each pyramid shares its basal plane corners with two *UU* tetrahedra from one silicate layer and two *DD* tetrahedra from an adjacent layer. The VO_5 pyramids appear to be disordered over two possible orientations, as typically occurring in the synthetic VSH family[15] (Figures 3 and 4).

The framework of VSH-2Cs contains two intersecting channel systems running along [011] and [0$\bar{1}$1] that are symmetry equivalent. These channels have a width defined by 8-membered rings (8MR) and a free aperture of 3.0×3.6 Å. A third system of channels runs along [010] that also has a free width of 3.0×3.6 Å. The Cs^+ ions and the water molecules occupy the voids within the channels in a zeolite-like fashion. The Cs cations are 12-fold coordinated, having an average bonding distance of 3.2 Å, with the shortest and longest distance being Cs2-O5 and Cs2-O6 at 2.856(6) and 3.466(7) Å, respectively.

The exchange of Cs^+ by Li^+ introduces a certain amount of inner strain that leads to fracturing of the crystals. Considering the crystal morphology, the orientation of the fractures is

Research Article
doi.org/10.1002/ejic.202300343

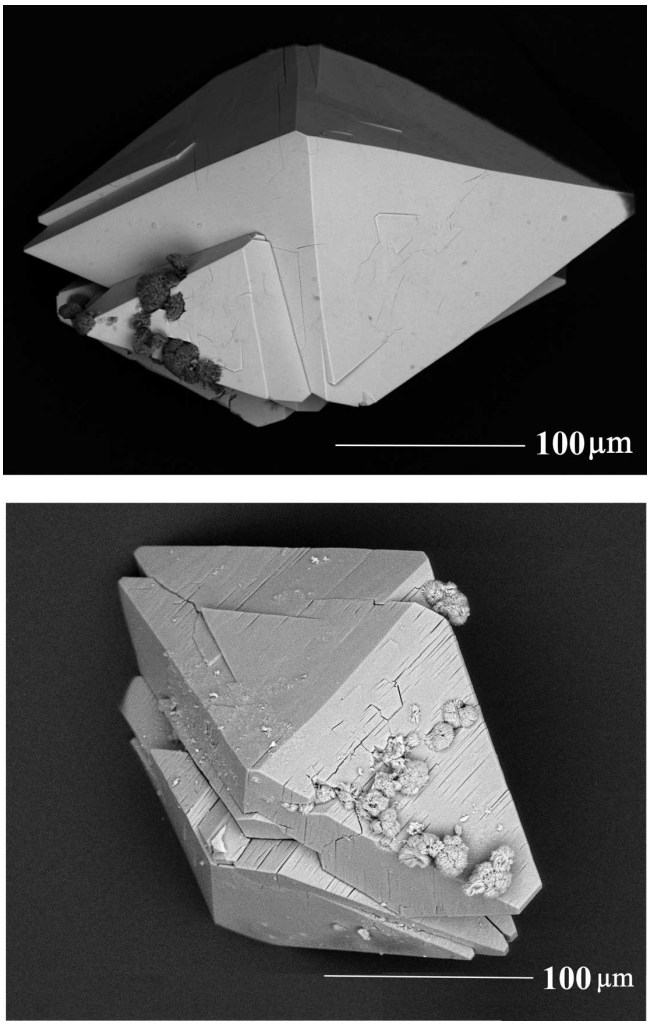

Figure 1. Scanning electron microscope (SEM) images of VSH-2Cs crystals as synthesized (above) and VSH-2Li (below).

perpendicular to the **a** axis and ions can diffuse only in the [011] layer (Figure 1). Therefore, the ion-transport is 2D since ions are hindered to move through the silicate tetrahedral layers. At the atomic scale, the replacement of Cs^+ by Li^+ leads to a significant distortion of the vanadosilicate framework. The unit-cell volume increases only slightly by 1.5% accompanied by lengthening of the **b** and **c** axes and shortening of the **a** axis (see Table 1). The symmetry appears to be monoclinic and the space group is *C*2/*c*, with monoclinic *ß* angle close to 90°, *ß* = 91.677(4)°. The change of symmetry is associated with slight rotations of polyhedra, but the topology of the framework remains intact. There is an increase of ellipticity of the 8MR along [010] while the deviation of the 6MR from circular decreases (Figures 2, 4). The shape of the 8MR along the **b** axis becomes more oblate with L/S = 1.58 compared to the as synthesized form with L/S = 1.35 (Figure 3).

Despite the obvious difference in unit-cell parameters, we attempt to quantify the degree of similarity between VSH-2Cs and VSH-2Li, neglecting the H_2O molecule sites in the calculation. The program STRUCTURE RELATIONS from the Bilbao Crystallographic Server was employed.[21] For the given structures, the degree of lattice distortion *S*, that is, the spontaneous strain obtained from the eigenvalues of the finite Lagrangian strain tensor calculated in a Cartesian reference system, has a value of *S* = 0.0094. The calculations revealed the following atomic displacements (in Å) between the corresponding atoms in VSH-2Cs as synthesized and VSH-2Li: Cs1/Li1: 1.3918; V1: 0.1675; Si1A: 0.3944; Si1B: 0.4171; Si2A: 0.5097; Si2B: 0.4584; O1A: 0.4498; O1B: 0.9066; O2: 0.3271; O3A: 0.8910; O3B: 0.3987; O4A: 0.6659; O4B: 0.6142; O5: 0.7417, therefore the maximum displacement is 1.3918 Å. The measure of similarity (Δ) as defined by Bergerhoff et al.[22] has a value of 0.121. Thus, this phase transformation seems to induce significant distortions of the vanadosilicate framework, as confirmed also by the increase of the average T-O-T angles from 141.3 to 147.1° (see Table S4).

The mechanism of framework distortion in VSH-2Li is not simply confined to a change in the T-O-T angles. To maintain chemically reasonable framework bond distances, there are concerted distortions of the ring systems. The strong interactions between Li ions and oxygen-framework atoms drive the main deformation mechanism, which is based on cooperative rotation of SiO_4 and VO_5 units around their oxygen atoms that behave as hinges. In particular, the four-connected *Q* tetrahedra rotate clockwise while the VO_5 pyramids rotate anticlockwise leading to the distortion of the tetrahedral layers (Figures 5 and 6). Moreover, the apical V=O groups are redirected and aligned parallel to the **b** axis in VSH-2Li (Figure 5).

The V site exhibits the most significant bond-length distortion index (Table 6). The increased distortion occurring at the V site after Li-exchange derives from the strain produced by the increased electronegativity of the Li counter-cation. The oxygen atoms shared with the Li cations have shorter bond lengths $<V–O>$ = 1.94 Å compared to the unshared ones with $<V–O>$ = 1.98 Å. Charge density calculations reveal that also the positive charge of the V site is increased indicating a lower charge transfer from the O^{2-} ligands to the V-atom. Finally, the low ECoN-values for the V site ranging from 3.75 to 2.76 indicate that the formal five-fold coordination is more adequately described as a 4 + 1 coordination.

Concerning the extraframework sites, the assignment of Li^+ at the Li1 site was possible by considering the short Li–O distances compared to Cs–O bond lengths. Li^+ occupies a pocket of the large Cs1 coordination polyhedron, due to the substantially smaller ionic radius, and is only 4-fold coordinated by oxygen atoms.

In particular, the Li1 is bonded to two framework oxygen atoms and two H_2O molecules. The Li-OW distances are on average 1.88 Å, while the Li–O distances are on average 1.87 Å (see Table S3). These observations match with the literature since Li polyhedra show often large variations of individual Li–O distances within the average $<Li–O>$ = 2.15 Å.[23] Refinement of Li^+ occupancy shows that the site is only half occupied with occupancy factor 0.48(5). Such amount would counterbalance only one of the two formal negative charges of the framework. The Li^+ cation binds to the basal oxygen atoms of the VO_5 pyramid as shown in Figure 7. As a result of its high

Research Article
doi.org/10.1002/ejic.202300343

Table 1. Experimental details.

Crystal data		
Sample	VSH-2Cs	VSH-2Li
Chemical formula	$Cs_2(VO)Si_6O_{14}\cdot 3H_2O$	$Li_{0.93}(VO)Si_6O_{14}\cdot 3H_2O$
M_r	779.35	514.42
Crystal system, space group	Orthorhombic, *Cmca*	Monoclinic, *C*2/*c*
T [K]	296	296
a, *b*, *c* [Å]	17.1174(3), 8.6958(1), 12.4430(2)	17.011(2), 8.8533(11), 12.4934(16)
ß [°]		91.677(4)
V [Å^3]	1852.13(5)	1880.7(4)
Z	4	4
Radiation type	Mo *Kα*	Mo *Kα*
Crystal size [mm]	0.1×0.05×0.05	0.05×0.05×0.03
Data collection		
Diffractometer	Bruker D8 Quest	Bruker D8 Quest
Absorption correction	Multi-scan (SADABS, [48])	Multi-scan (SADABS, [48])
No. of measured, independent and observed [$I > 2\sigma(I)$] reflections	28437, 2298, 2243	15630, 2883, 1672
R_{int}	0.023	0.076
$(\sin\theta/\lambda)_{max}$ [Å^{-1}]	0.834	0.715
Refinement		
$R[F^2 > 2\sigma(F^2)]$, $wR(F^2)$, *S*	0.021, 0.059, 1.26	0.116, 0.363, 1.14
No. of reflections	2298	2883
No. of parameters	90	128
No. of restraints	–	2
$\Delta\rho_{max}$, $\Delta\rho_{min}$ [e Å^{-3}]	1.01, −0.38	1.90, −0.67

Computer programs: *SHELXL2018*/3

Table 2. Atomic coordinates and U_{iso} values for VSH-2Cs.

Site	Atom	Occ.[a]	*x*	*y*	*z*	U_{iso}
Cs1	Cs	0.5	0.000000	0.1310(3)	0.3114(2)	0.0310(4)
Cs2	Cs	0.3139	0.000000	0.1371(6)	0.2927(3)	0.0359(6)
Cs3	Cs	0.1861	0.000000	0.1096(8)	0.3207(7)	0.0450(14)
Si1	Si	1	0.250000	0.20284(4)	0.250000	0.00830(7)
Si2	Si	1	0.16713(2)	0.45763(3)	0.38643(2)	0.00838(6)
V1	V	0.5	0.000000	0.55320(6)	0.48396(4)	0.00937(8)
O1	O	1	−0.18279(6)	0.09652(11)	0.19825(7)	0.01808(15)
O2	O	1	0.20996(6)	0.500000	0.500000	0.01413(18)
O3	O	1	0.21059(6)	0.30553(10)	0.34178(7)	0.01956(16)
O4	O	1	0.07607(5)	0.43232(11)	0.39974(6)	0.01592(14)
O5	O	0.5	0.000000	0.7228(3)	0.4288(2)	0.0220(5)
O6	O	0.5	−0.1190(2)	0.9507(6)	0.4766(5)	0.0778(18)
O7	O	0.25	−0.0433(11)	0.816(2)	0.4170(13)	0.134(6)

[a] Occupancies of Cs sites were initially refined but fixed in the final cycles.

charge density, the Li^+ binds only on one side of the basal oxygen atoms of VO_5 while Cs^+ is present of both sides. Such incomplete exchange reaction arises from the impossibility to accommodate the Li^+ cations with the negative charge distribution on the host framework. Therefore, it is highly probable that charge-balancing protons are present combined with water molecules as H_3O^+ or $H_5O_2^+$.

Research Article
doi.org/10.1002/ejic.202300343

Table 3. Atomic coordinates and U_{iso} values for VSH-2Li.

Site	Atom	Occ.[a]	*x*	*y*	*z*	U_{iso}
Si1A	Si	1	0.500000	0.4992(3)	0.750000	0.0201(6)
Si1B	Si	1	0.500000	0.0018(3)	0.750000	0.0188(6)
Si2A	Si	1	0.40708(11)	0.2492(3)	0.36108(15)	0.0183(4)
Si2B	Si	1	0.42811(11)	0.2509(3)	0.59657(15)	0.0185(4)
V1	V	0.5	0.25008(19)	0.1926(3)	0.5029(2)	0.0201(5)
O1A	O	1	0.5699(4)	0.6038(7)	0.7076(5)	0.0335(15)
O1B	O	1	0.4652(4)	0.1026(7)	0.6529(5)	0.0334(15)
O2	O	1	0.4577(3)	0.2497(7)	0.4739(4)	0.0233(11)
O3A	O	1	0.4300(4)	−0.1007(7)	0.7932(5)	0.0305(14)
O3B	O	1	0.4642(4)	0.3995(8)	0.6544(5)	0.0363(15)
O4A	O	1	0.3144(3)	0.2492(8)	0.3792(4)	0.0283(12)
O4B	O	1	0.3354(3)	0.2495(9)	0.5992(5)	0.0369(16)
O5	O	0.5	0.2482(8)	0.0179(17)	0.5121(12)	0.042(3)
Li1	Li	0.4814	0.231(2)	0.274(3)	0.282(2)	0.035(7)
OW1	O	0.5	0.3640(15)	−0.231(3)	0.525(2)	0.079(6)
OW2	O	0.5	0.2436(14)	0.411(3)	0.1759(18)	0.082(4)
OW3	O	0.5	0.1851(15)	0.156(3)	0.1642(19)	0.082(4)

[a] Occupancies of Li sites were initially refined but fixed in the final cycles.

Table 4. Anisotropic displacement parameters for VSH-2Cs.

Site	U^{11}	U^{22}	U^{33}	U^{23}	U^{13}	U^{12}
Cs1	0.0352(5)	0.0265(4)	0.0315(11)	−0.0082(6)	0.000	0.000
Cs2	0.0255(4)	0.0386(11)	0.0435(14)	−0.0224(11)	0.000	0.000
Cs3	0.0529(17)	0.049(3)	0.0335(11)	−0.0029(14)	0.000	0.000
Si1	0.01043(14)	0.00657(13)	0.00790(13)	0.000	0.00108(11)	0.000
Si2	0.00818(11)	0.00970(11)	0.00726(10)	−0.00202(7)	0.00152(7)	−0.00105(8)
V1	0.00755(16)	0.01313(18)	0.00744(16)	−0.00098(13)	0.000	0.000
O1	0.0178(3)	0.0182(3)	0.0183(3)	−0.0070(3)	0.0001(3)	0.0058(3)
O2	0.0106(4)	0.0227(5)	0.0091(4)	−0.0057(3)	0.000	0.000
O3	0.0250(4)	0.0158(3)	0.0178(3)	−0.0074(3)	0.0045(3)	0.0049(3)
O4	0.0096(3)	0.0252(4)	0.0130(3)	−0.0058(3)	0.0025(2)	−0.0041(3)
O5	0.0279(12)	0.0179(10)	0.0202(11)	0.0047(8)	0.000	0.000
O6	0.0391(17)	0.090(4)	0.104(5)	0.035(3)	0.012(2)	0.0157(18)

Symmetry mode analysis of the phase transformation

Diffraction experiment point to a *translationengleiche* phase transition of index 2. The space groups *Cmca* (high symmetry) and *C2/c* (low symmetry) are in group-subgroup relationship and the crystal structures have similar topological features. The atomic coordinates of the high- and low-symmetry structures are related by the following transformation (***P***,*p*): (−**a**, **b**, −**c**;−1/4, 1/4, −1/2).

A more exhaustive understanding of the phase transformation induced by Li-ion exchange can be achieved by symmetry-mode analysis. We use the program AMPLIMODES[24] that allows the decomposition of the structural distortions present in the low-symmetry structure into contributions from different modes, whose symmetries are given by the irreducible representations (irreps) of the space group of the high symmetry phase.

The phase transformation decomposes into two distortion modes of different symmetry corresponding to the irreps Γ_1^+ and Γ_4^+. The fully symmetrical Γ_1^+ distortion retains the symmetry of the *Cmca*-structure, while Γ_4^+ represents the symmetry-breaking structural distortion. In a first step, a reference structure representing the parent phase in the low-symmetry C2/c space groups (see Table S5) was calculated ignoring the extraframework water sites due to incompatibility with respect to the Wyckoff positions splitting. The resulting displacement field was then obtained from the comparison of the reference structure with the low symmetry phase (see

Research Article
doi.org/10.1002/ejic.202300343

Table 5. Anisotropic displacement parameters for VSH-2Li.

Site	U^{11}	U^{22}	U^{33}	U^{23}	U^{13}	U^{12}
Si1A	0.0285(16)	0.0135(13)	0.0185(13)	0.000	0.0035(11)	0.000
Si1B	0.0244(15)	0.0134(13)	0.0183(12)	0.000	−0.0024(10)	0.000
Si2A	0.0194(8)	0.0193(9)	0.0163(8)	−0.0002(8)	0.0017(6)	−0.0007(9)
Si2B	0.0207(9)	0.0193(9)	0.0154(8)	0.0000(8)	−0.0006(6)	−0.0009(9)
V1	0.0195(10)	0.0237(10)	0.0172(10)	−0.0008(11)	0.0018(8)	0.0008(13)
O1A	0.035(4)	0.030(3)	0.035(3)	0.009(3)	−0.001(3)	−0.013(3)
O1B	0.047(4)	0.022(3)	0.031(3)	0.012(2)	−0.004(3)	0.009(3)
O2	0.019(2)	0.032(3)	0.019(2)	0.002(2)	−0.0008(17)	0.009(3)
O3A	0.032(3)	0.031(3)	0.029(3)	0.014(2)	−0.001(2)	−0.007(3)
O3B	0.044(4)	0.032(3)	0.033(3)	−0.009(3)	0.000(3)	−0.001(3)
O4A	0.018(2)	0.046(3)	0.021(2)	0.000(3)	0.0011(18)	−0.006(3)
O4B	0.019(2)	0.073(5)	0.019(2)	0.011(3)	0.0010(19)	−0.001(3)
O5	0.041(7)	0.040(8)	0.045(8)	0.026(6)	0.008(6)	−0.004(7)

Table 6. Charge Distribution (CD) and Bond Valence (BV) for VSH-2Cs and VSH-2Li.

	BV	CD	ECoN	c.n.	Distortion index	Polyhedral volume Å^3
Cs	1.02	1.00	9.14	12	0.0375	61.6536
V	3.90	3.97	3.75	5	0.0567	5.1016
Si1	4.02	3.96	4.00	4	0.0035	2.1183
Si2	3.94	4.17	3.98	4	0.0098	2.1554
Li	1.08	0.99	3.88	4	0.02455	2.7140
V	4.01	4.17	2.76	5	0.06875	4.8622
Si1A	4.02	4.02	3.99	4	0.00537	2.1006
Si1B	3.98	4.02	4.00	4	0.00059	2.1158
Si2A	3.93	3.99	3.99	4	0.00553	2.1613
Si2B	3.99	4.25	3.98	4	0.00895	2.1275

Table 7). The vectors **u** for the atoms of the reference structure define the displacive distortions relating both structures. As already mentioned previously, the maximum displacement parameter is 1.3918 Å and relates to the dislocation of extraframework cation site. The silicon and oxygen atoms are distinctly affected by the phase transformation and their absolute shifts vary between 0.327 and 0.907 Å. In contrast, the vanadium atom site shows a considerably smaller displacement of 0.168 Å. The average displacement of all corresponding atom pairs in both structures has a value of 0.6159 Å.

In the following step of the symmetry-mode analysis, the absolute amplitudes for the two components of the global distortions were calculated: the values are 4.3551 Å for Γ_1^+ and 2.2916 Å for Γ_4^+. The Γ_1^+ mode is about 2 times larger, indicating that this non-symmetry breaking mode gives a fundamental contribution to the onset of the transition. To obtain a graphical overview of the distortion fields, the polarization vectors for each involved irrep were calculated. Table S6 lists the crystallographic description of these normalized vectors. From examination of Table S6, it is clear that the displacement vectors of the most affected atoms possess parallel or antiparallel orientation with respect to the layers (100) for the Γ_1^+ and (010) for the Γ_4^+ representations. The graphical description of the individual displacements related to Γ_1^+ and Γ_4^+ are given in Figures 5 and 6, respectively. The figures depict in (a) the graphical description of the shifts which are attributed to the most affected atoms (Cs1/Li1, O1, O3, O5 for the Γ_1^+-mode and Cs1/Li1, Si2, O1, O3 and O4 for the Γ_4^+-mode), while in (b) is represented the virtual structure given in the subgroup basis in which only the symmetry modes compatible with the respective irrep are frozen.

The Γ_1^+-mode distortion pattern appears to be dominated by three features: (i) alignment along [010] of the vanadyl groups driven by the shifting of the apical O5 oxygen atom; (ii) displacement of the Cs1/Li1 sites closer to the VO_5 pyramids; (iii) adjustment of the 4-membered ring aperture by opposite shifts of the O1 and O3 framework oxygen atoms.

The Γ_4^+ representation is characterized by: (i) clockwise rotation of the oxygen atoms (O1 and O3) coordinated to Si1, movement accompanied also by the surrounding Si2 sites (ii) anti-clockwise rotation of the O4 sites that constitute the basal oxygen atoms of the square-based VO_5 pyramids (iii) mutually antiparallel shifts of the O2 sites belonging to the same six-membered ring which basically increase the Si2-O2-Si2 angle (see Table S4). (iv) displacement of the Cs1/Li1 site strictly parallel or antiparallel to [100].

Hydrogen-bond network and protonated water clusters

The arrangement of the water molecules in the structural channels is significantly different in VSH-2Cs and VSH-2Li. The observed differences in the coordination spheres of the cations can be explained in terms of hydration energy. The smaller Li^+ ions have higher charge density on their surface than the larger Cs^+ cations and, therefore, the hydration energy of Li^+ is higher. The H_2O molecules are strongly bonded to Li^+ with

Research Article
doi.org/10.1002/ejic.202300343

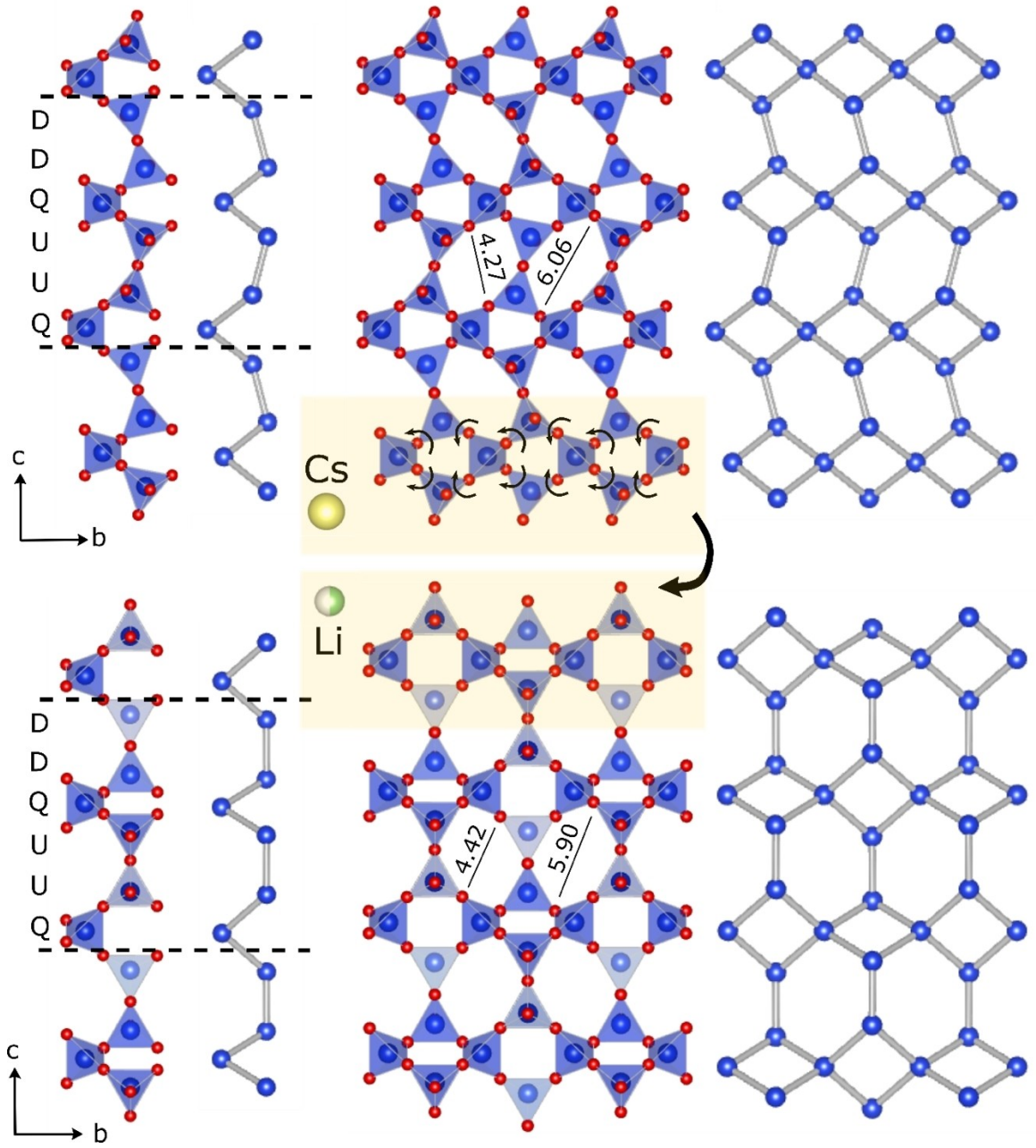

Figure 2. Single chain and sheet in VSH-2 consisting of [SiO_4]-tetrahedra parallel to [001] represented by polyhedra, and ball-and-stick model, diameters of the 6MR are in Å.

$<$Li-OW$>$ = 1.88 Å while for Cs^+ $<$Cs-OW$>$ = 3.29 Å. However, it remains enigmatic how the Li^+ cations diffuse through the narrow 8MR windows in VSH-2 structure: does the Li-ion diffuse with its coordinating water shell or is the water stripped off to allow the passage in the narrow 8MR?

In VSH-2Cs, H_2O molecules in the structural channels at O6 and O7 sites are adsorbed exclusively in the vicinity of the Cs^+ extraframework site and coordinated to those cations. Two kinds of adsorbed water molecules are instead distinguished in VSH-2Li: 1) H_2O molecules (OW2 and OW3 sites) in the vicinity of Li^+ bonded to these extra-framework cations 2) H_2O molecules (OW1 site) adsorbed in other parts of the accessible pore space that are not strongly bonded to any atom but interact with their environment exclusively through hydrogen bonds. The latter molecules can be defined as "space fillers" since they are not coordinated to any cation but linked by hydrogen bonds to the cavity surface.

The O–H stretching region in the wavelength range 4000 to 3000 cm^{-1} of the FTIR spectrum of VSH-2Cs is characterized by two peaks at 3566, 3460 cm^{-1}, and a shoulder at 3306 cm^{-1} (Figure 8). According to the hydrogen-bond-length versus IR frequency correlation by Libowitzky[25] absorptions between 3460 and 3566 cm^{-1} correspond to donor–acceptor distances of ca. 2.9–3.5 Å which agrees with the D–A distances in Table 8.

Research Article
doi.org/10.1002/ejic.202300343

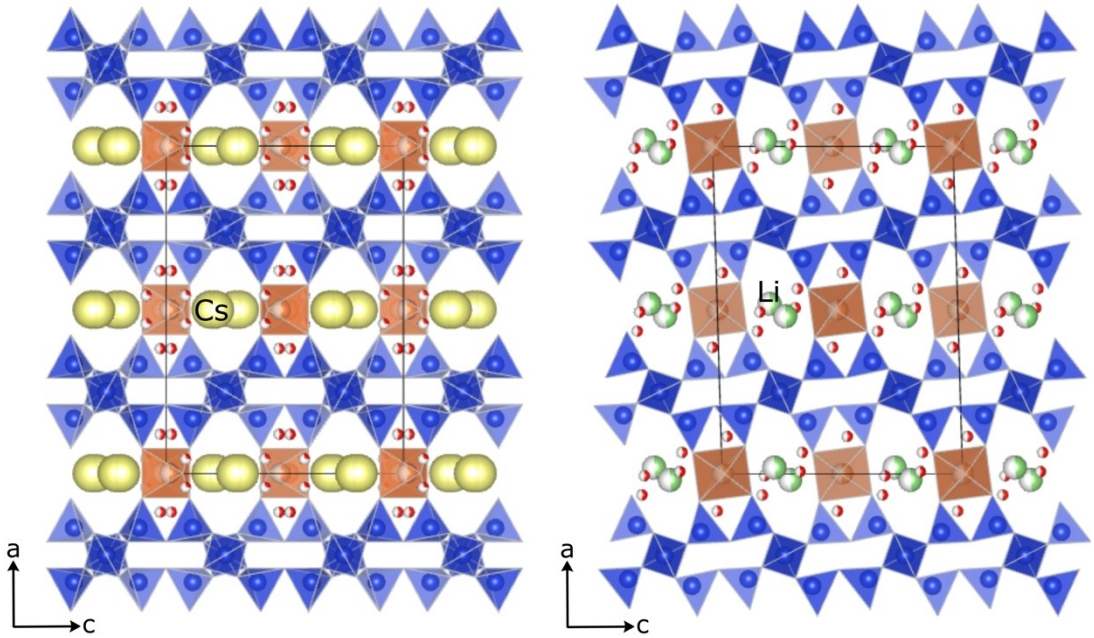

Figure 3. Framework structure of VSH-2Cs as synthesized (on the left) and VSH-2Li exchanged (on the right). The blue polyhedra represent SiO_4 tetrahedra, while the orange polyhedra are the $V^{4+}O_5$ pyramids. Cesium cations are in yellow, lithium in green and oxygen of H_2O are shown as red spheres.

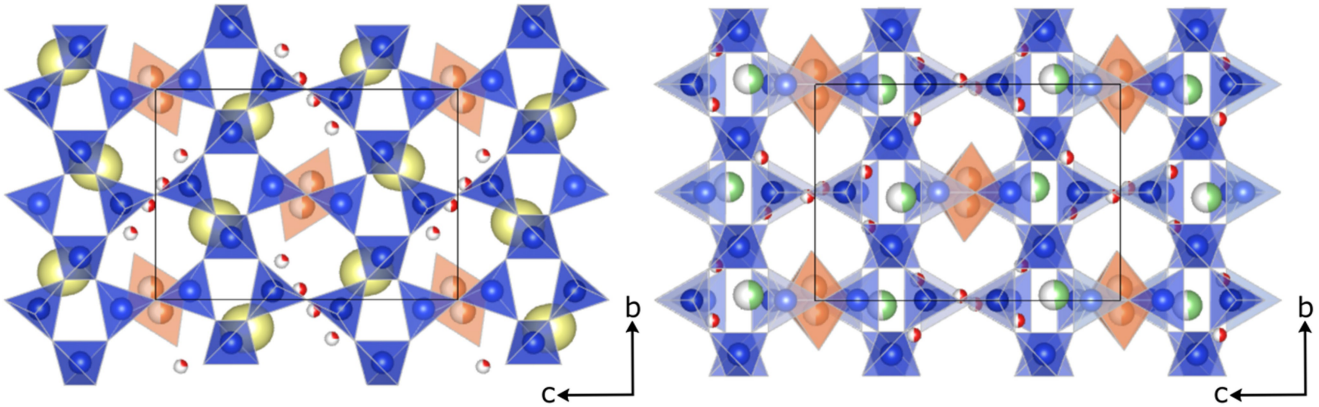

Figure 4. Tetrahedral layer of VSH-2Cs as synthesized (a) and Li-exchanged (b) in monoclinic C2/c. Cesium cations are in yellow, lithium in green and oxygen of H_2O are shown as red spheres.

The shoulder at 3306 cm^{-1} corresponds to donor–acceptor distances of 2.7–2.8 Å.[25] Such strong hydrogen bond was observed in terms of D–A distance for *d*(O7…O6) and *d*(O5…O6). The DFT-calculated IR-active modes for the $Cmc2_1$ ordered model of VSH-2Cs are matching well with the experimental IR-active modes (Figure 8).

The O–H stretching region of the FTIR spectrum of VSH-2Li shows two peaks at 3557, 3409 and a shoulder at 3246 cm^{-1} (Figure 8). Compared to the spectrum of VSH-2Cs, there is a shift to lower frequencies (red shift) of the FTIR modes. Hydrogen bonding leads to a weakening of the primary covalent O–H, thus shorter hydrogen bonds result in a decrease in frequency of the FTIR peaks. This observation agrees with the presence of shorter hydrogen-bonds in VSH-2Li, in particular the *d*(OW1…OW3) and *d*(OW2…O5) have a D–A distance of 2.68(4) and 2.54(3), respectively (Table 8). The DFT-calculated IR-modes present some additional modes at low wavenumbers (Figure 8). However, not all the tick marks in Figure 8 necessarily correspond to visible bands because some modes may have near-zero intensity (the DFT results do not contain any intensity information).

To visualize the hydrogen bonding scheme of the H_2O molecules and coordination environment of the extraframework cations, we obtained two DFT-optimized structures. Both structures were optimized after removing the disorder. Model *a* represents the case in which the Li fully occupies the extraframework positions, while the model *b* illustrates the alkali deficient framework with formation of protonated species (Figure 9). In the first model, there are two crystallographically independent OW1 sites that are hydrogen bonded to the framework oxygen atoms and water molecules with D–A distances between 2.769 and 3.269 Å, which agrees well with

Research Article
doi.org/10.1002/ejic.202300343

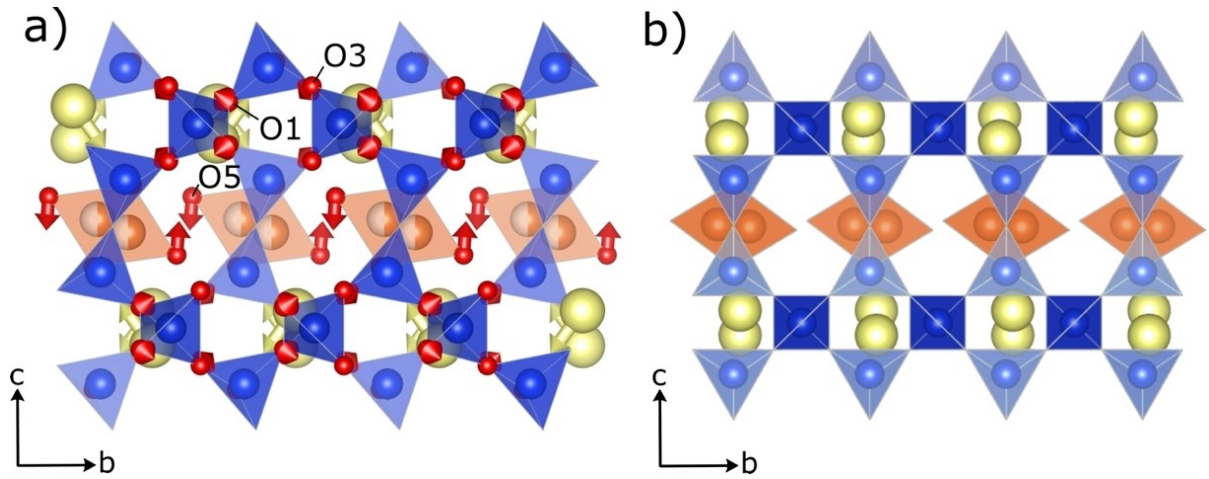

Figure 5. Displacement field induced by the Γ_1^+ component on the reference structure. (a) Description of the shifts of the most affected atoms. The directions of the atomic displacements correspond to the directions of the arrows. For sake of better visibility, the lengths of the arrows have been scaled to a common factor. (b) Virtual structure given in the subgroup basis in which only the symmetry modes compatible with the Γ_1^+ irrep are frozen.

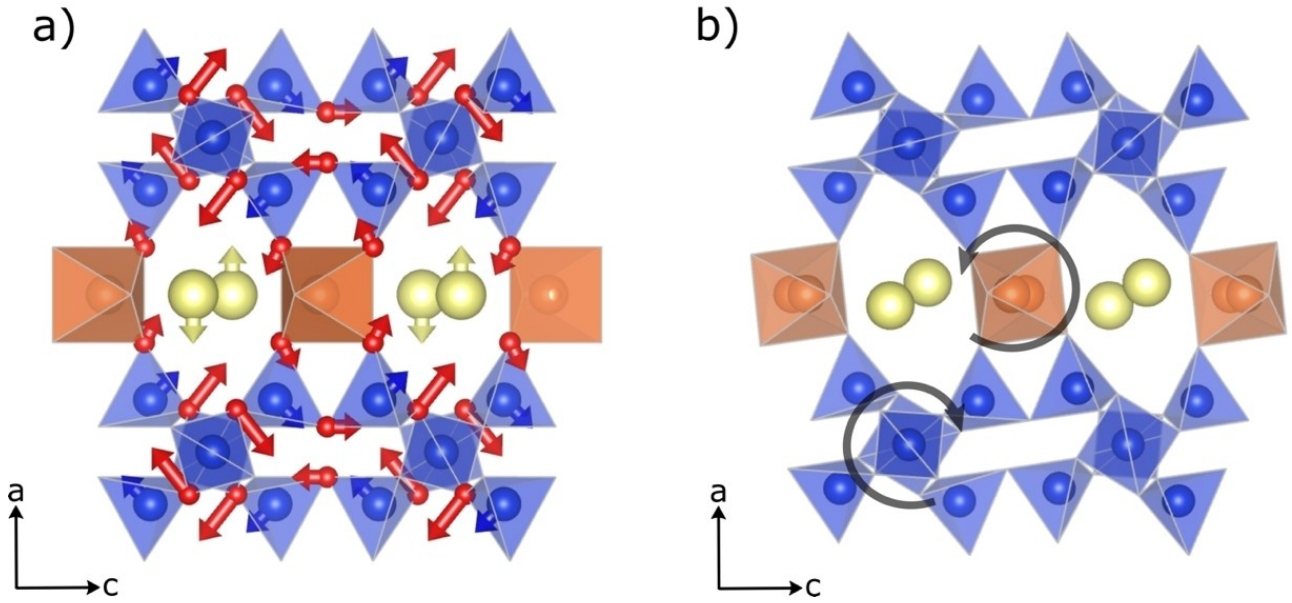

Figure 6. Displacement field induced by the Γ_4^+ component on the reference structure. (a) Description of the shifts of the most affected atoms. The directions of the atomic displacements correspond to the directions of the arrows. For sake of better visibility, the lengths of the arrows have been scaled to a common factor. (b) Virtual structure given in the subgroup basis in which only the symmetry modes compatible with the Γ_4^+ irrep are frozen.

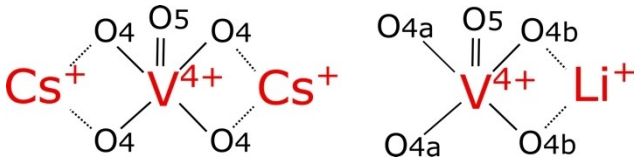

Figure 7. Schematic representation illustrating the binding of charge-balancing alkali ions with the basal oxygen atoms of the square-based VO_5 pyramid for the case of Cs^+ and Li^+.

the experimental data (see Table S1). In contrast, OW2 and OW3 sites are bonded to the Li-cations and involved in a hydrogen bonding scheme with D–A distances between 2.708 and 2.979 Å, which diverges significantly from the experimental distances due to the readjustments of the H_2O positions in the optimization.

In the second model, the incomplete Li^+ substitution at the extraframework sites was considered. Exchange of Cs^+ by Li^+ is accompanied by the formation of protonated species to counterbalance the framework net negative charge. Although the size of protonated clusters remains highly debated in the literature, there is a general agreement that the protonated water dimer is the most stable equilibrium structure.[26] Thus, the charge-balancing protons are combined with the H_2O molecule to form preferentially $H_5O_2^+$ groups.

In VSH-2Li, the most suitable candidate for the protonation state is the "space filling" H_2O molecule at the OW1 site. This hypothesis is corroborated by suitable OW1-O bond lengths

Research Article
doi.org/10.1002/ejic.202300343

Table 7. Displacement field for the low-symmetry *C2/c*-phase.

Atom	Atomic Displacements			
	u_x	u_y	u_z	|u|
Cs1 (Cs1/Li1)	−0.0190	−0.1131	0.0747	1.3918
Si1 (Si1A)	0.0000	0.0454	0.0000	0.3944
Si1_2 (Si1B)	0.0000	−0.0480	0.0000	0.4171
Si2 (Si2A)	0.0100	0.0416	0.0254	0.5097
Si2_2 (Si2B)	0.0110	−0.0415	−0.0170	0.4584
V1 (V1)	0.0001	0.0042	−0.0131	0.1675
O1 (O1A)	−0.0027	0.0497	−0.0094	0.4498
O1_2 (O1B)	−0.0324	−0.0509	0.0454	0.9066
O2 (O2)	0.0023	−0.0004	0.0261	0.3271
O3 (O3A)	0.0306	0.0452	0.0486	0.8910
O3_2 (O3B)	0.0036	−0.0450	−0.0038	0.3987
O4 (O4A)	0.0117	0.0669	0.0205	0.6659
O4_2 (O4B)	0.0093	−0.0682	−0.0011	0.6142
O5 (O5)	−0.0018	0.0093	−0.0592	0.7417

u_x, u_y nd u_z are given in relative units. |u| is the absolute displacement in Å. Wyckoff splittings are indicated using underscore signs, e.g. Si1_2. Labels in parenthesis refer to nomenclature of the positions used in the low-symmetry phase.

with O…O distances from 2.44 to 3.5 Å.[27] The most probable hydrogen bonds involve OW1…OW3 = 2.658 Å, OW1…O2 = 3.031 Å and OW1-O5 = 2.936 Å, in agreement with the experimental data. The H_3O^+ group at OW1 site is therefore hydrated to form $H_5O_2^+$ since the OW3 position is a water site. Hydrogen bonds to H_2O molecules appear to be necessary to stabilize the proton at OW1 in VSH-2Li. In particular, the strong OW1…OW3 hydrogen bonding is the closest water ligand of the hydration shell denoted as "special pair".[28] Such ligand suggests the dominant role of the water-water interactions to maintain the protonation state. Therefore, the role of OW1 is not only crucial in filling the void left by the exchange of larger Cs^+ by Li^+ but also mediate proton transfer to compensate the negative charge of the host vanadosilicate framework. The hypothetical removal of the protonated water dimers would decrease the Li coordination number to a critical level leading to the collapse of the VSH-2 framework. The Li limiting coordination number should be 3.[29]

Concerted influence of microstructure, low framework charge density and adsorbed H_2O molecules seem to determine the Li-ion exchange mechanism. The strong hydrogen bonding between the H_2O molecules is essential for the proton-transfer process from the framework to the water dimer. The formation of protonated water dimers is inferred in VSH-2Li but remains one of the most elusive species for direct structural characterization by experimental methods due to its chemical similarity to H_2O.[30] The favorability of the substitution of protons for lithium in vanadosilicate frameworks compounds hinges on the ability of the structure to form protonated species without severely degrading the bonding of the rest of the structure by distorting the coordination polyhedra of the framework.

Finally, the study of vanadosilicate VSH-2 helps us in understanding the ion-exchange mechanisms and the accompanying hydration process. The characterization of the water in confined porous environments appears to be critical for a molecular description of ion-exchange mechanisms. In future studies, we are aiming to further investigate the role of protonated water clusters in ion-exchange processes of porous frameworks.

Conclusions

The influence of Li substitution on the open framework vanadium silicate VSH-2Cs has been examined by means of SCXRD, ATR-FTIR and DFT calculations. Cooperative rotation of SiO_4 and VO_5 units in response to Li-ion exchange led to changes in the lattice parameters and reduction of the orthorhombic symmetry (*Cmca*) to monoclinic (*C2/c*). The distortion pattern has been studied using group-theoretical

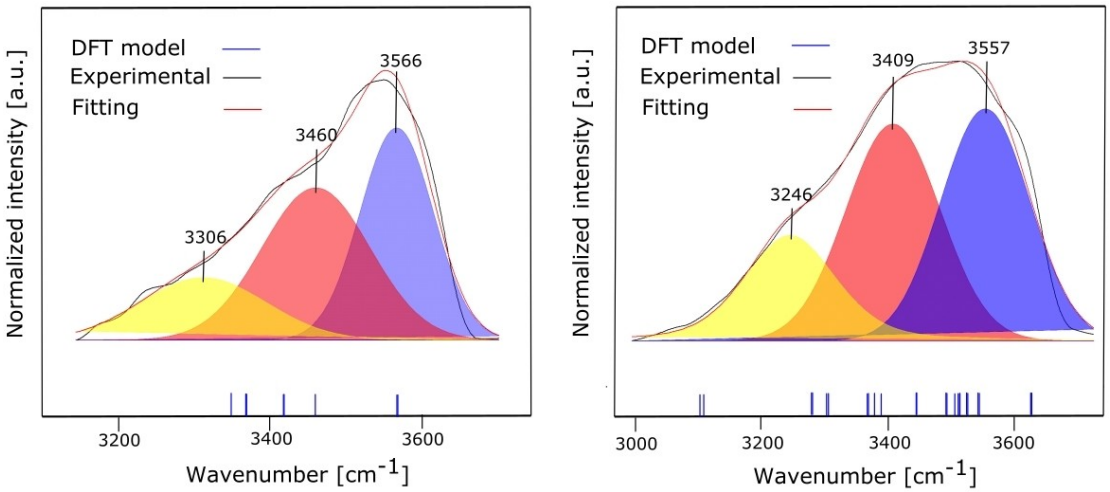

Figure 8. ATR-FTIR spectra of VSH-2Cs and VSH-2LI. The black curve is the experimental, in red the fitting. In blue are reported the peaks from the DFT model.

Research Article
doi.org/10.1002/ejic.202300343

Table 8. Hydrogen bond distances and angles in VSH-2Cs and VSH-2Li with hydronium.

	VSH-2Cs			VSH-2Li hydronium	
	SCXRD	DFT		SCXRD	DFT
O6			**OW1**		
d(O6…O5)	3.278 (6) Å	2.841 Å	*d*(OW1…OW3)	2.68(4) Å	2.658 Å
d(H1…O4)		1.902 Å	*d*(H1…OW3)		1.606 Å
α(O6-H1…O4)		158.1°	α(OW1-H1…OW3)		174.6°
d(O6…O2)	2.928 (4)	3.128 Å	*d*(OW1…O2b))	3.0(3) Å	3.031 Å
d(H2…O2)		2.181 Å	*d*(H2…O2b)		2.051 Å
α(O6-H2…O2)		163.0°	α(OW1-H2…O2b)		164.4°
			d(OW1…O5)	2.96(3) Å	2.936 Å
			d(H3…O5)		1.969 Å
			α(OW1-H3…O5)		159.0°
O7			**OW2**		
d(O7…O6)	2.747 (2) Å	2.824 Å	*d*(OW2…O5)	2.54(3) Å	2.518 Å
d(H3…O6)		1.881 Å	*d*(H4…O5)		1.620 Å
α(O6-H3…O6)		159.4	α(OW2-H4…O5)		148.8°
d(O7…O6)	2.747 (2) Å	2.824 Å	*d*(OW2…O4b)	3.53 (3) Å	3.211 Å
d(H4…O1)		1.881 Å	*d*(H5…O4b)		2.435 Å
α(O7-H4…O1)		159.4	α(OW2-H5…O4b)		135.74
			OW3		
			d(OW3…O1d)	3.08 (3) Å	3.044 Å
			d(H6…O1d)		2.057 Å
			α(OW3-H6…O1d)		172.7°
			d(H7…)		No acceptor found

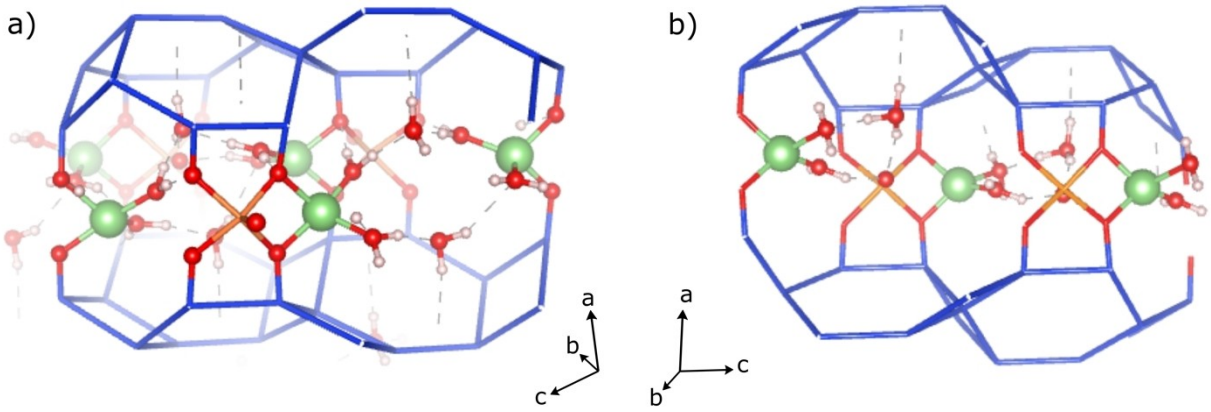

Figure 9. Skeletal representation of the DFT-optimized structures with focus on the Li coordination. Lithium cations are in green, H_2O molecules in red and hydrogen atoms in white. Hydrogen bonds are represented as dashed lines.

methods including mode analysis. The Cs sites are converted into new distorted tetrahedral sites for smaller Li^+ ions via 2D ion transport along the [011] direction. Exchange of Cs^+ by Li^+ is incomplete suggesting the formation of protonated H_2O species to counterbalance the net negative framework charge. These findings demonstrate the importance of the formation of a favorable coordination environment for the stability of extraframework cations in zeolites.

Analytical methods

Material synthesis

VSH-2Cs sample material was synthesized by hydrothermal methods following the published protocol.[14] Blue crystals partially covered by whitish particles of unreacted silica where recovered by filtration. The yield is ~60%. Subsequently, the crystals were washed with deionized water to remove the amorphous particles. The crystalline material appears as distorted octahedral VSH-2Cs

Research Article
doi.org/10.1002/ejic.202300343

crystals (Figure 1). Energy dispersive X-ray (EDX) analysis shows the framework components V, Si and O with additional Cs as extraframework cations in agreement with previously reported data[14] (Figure S1, in Supporting Information).

A crystal of approximate dimensions 0.10×0.05×0.05 mm was selected and mounted on a glass fiber to perform single-crystal X-ray diffraction. This first sample is denominated VSH-2Cs as synthesized.

Lithium ion-exchange experiment was carried out by stirring the as-synthesized crystalline sample in a large excess of exchanging ion in aqueous solution, following a procedure described elsewhere.[15] The sample was heated and stirred in 30 mL of a 1 M $LiClO_4$ solution at 323 K for 40 h and then washed with deionized water. The process was repeated another time to remove all possible residual Cs from the material. The crystals were then separated from the solution and found to be fractured and easily separable into several smaller pieces (Figure 1 and S2b, in Supporting Information). The EDX analysis gave 0% Cs compared to ~25% Cs for the as synthesized sample, suggesting complete exchange of Cs^+ by Li^+. The Cs is fully removed as extraframework component, residuals are from the recrystallized exchange solution, trapped in the interstices of the intergrown crystals. Thus, we selected a crystal of approximated dimensions 0.05×0.05×0.03 mm and mounted it on a glass fiber for further characterization. This second sample is denominated VSH-2Li exchanged.

Single Crystal X-ray Diffraction (SCXRD)

Single-crystal X-ray diffraction measurement of the two samples was performed on a Bruker D8 Quest diffractometer using $Mo_{K\alpha}$ radiation ($\lambda = 0.71076$ Å) at the Karlsruhe Institute of Technology, Department of Applied Geosciences. The instrument is equipped with a Mo-Microfocus IμS 3.0 and a Photon III area detector. The data were integrated and an empirical absorption correction was applied using the Apex 3 software package. Data-collection and refinement parameters for the two samples are listed in Table 1. Neutral atom scattering factors were used for structure refinement with SHELXL.[31] For the crystal structure refinement of VSH-2Cs as synthesized, we used the starting model of Wang et al.[14] The refinement of VSH-2Cs in the originally described *Cmca* space group converged to R1 values of ~0.02. This structural model is compatible with a disordered arrangement of the VO_5 pyramids over two positions that have the same basal plane and opposite apical vanadyl groups. Aiming to untangle the orientational disorder in VSH-2Cs, we derived from the *Cmca* structure two ordered models: polytype A with antiparallel orientation of the vanadyl groups in adjacent (001) layers and polytype B with all the vanadyl groups in adjacent layers oriented in the same way (Figure S3). Using the ADDSYM test by the program PLATON,[32] we could assign space group $Cmc2_1$ (Nr. 36) to polytype A and *Cm2a* (standard setting *Abm2*, Nr. 39) to polytype B. Both $Cmc2_1$ and *Cm2a* belong to the maximal non-isomorphic subgroups of *Cmca*. On a purely theoretical level, a twinned coherent intergrowth between the two polytypes would be compatible with a monoclinic structural model with space group *Cm* (Nr. 8) on the base of the common symmetry operators. However, when analyzing the systematic absences in our dataset, we could find only very weak forbidden reflections (*e.g.* 150, 350 systematically absent in *Cmca* and *Cm2a* or 401, 601 systematically absent in *Cmca* and $Cmc2_1$) but not all the symmetry related reflections with $I > 3\sigma(I)$. These indications are too faint to justify the choice of a lower-symmetry space group. Furthermore, any attempt to refine a lower symmetry structure failed to solve the splitting of the vanadium sites in two positions with occupancy of 0.50% and characterized by short V–V distances of about 1 Å. Thus, we maintain the *Cmca* model as best compromise to describe the topological symmetry of VSH-2Cs.

The structural distortions after lithium exchange lead to a lowering of the symmetry and according to the systematic absences space group *C2/c* was selected. Structure solution by direct methods and subsequent structure refinement in the monoclinic model for VSH-2Li converged to R1 values of about 0.11.

Atomic coordinates and displacement parameters for the VSH-2Cs and VSH-2Li are given in Tables 2–5. Selected bond distances and angles are reported in Table S3 while the T-O-T angles are listed in Table S4.

Deposition Numbers 2249699 (for VSH-2Cs) and 2249700 (for VSH-2Li) contain the supplementary crystallographic data for this paper. These data are provided free of charge by the joint Cambridge Crystallographic Data Centre and Fachinformationszentrum Karlsruhe Access Structures service.

To provide a quantitative estimate for the framework distortion upon lithium exchange we calculate the L/S ratio.[33] This ratio is measured between opposite oxygen sites along the longest (L) and shortest (S) cross sections of the eight membered rings. Figures showing structural features were prepared using the program VESTA.[34] The same program was also employed for the calculation of the effective coordination numbers (ECoN:[35]) as well as volume and distortion indices of the MOx-polyhedra which can be found in Table 6. To validate the refined structures, the bond valence calculations (BV)[36] and the charge distribution (CD) analysis[37] were applied and reported in Tables S2 and 6. The BV approach uses empirical correlations between the bond length and strength of chemical bonds, while the CD method distributes the formal oxidation number, q, of each atom among all its bonds as a function of a non–integer effective coordination number (ECoN).

Attenuated Total Reflection Fourier-transform Infrared Spectroscopy (ATR-FTIR)

The ATR-FTIR data have been collected using a Bruker Tensor 27 FTIR spectrometer with a Platinum-ATR unit on a diamond crystal in single reflection geometry. Analyses have been performed with single-crystal samples at wavenumbers between 400 cm^{-1} and 4000 cm^{-1}. Each sample was measured using 40 repetitions and then referenced to a background analysis in air. The spectra are corrected for a refractive index of n = 1.55 and a smoothing with 25 points was applied.

Density Functional Theory (DFT) calculation

DFT calculations were carried out with the CASTEP code, which uses a plane-wave pseudopotential approach.[38] In these calculations, the Perdew-Burke-Ernzerhof (PBE) exchange-correlation functional[39] was combined with the dispersion correction proposed by Tkatchenko and Scheffler (TS).[40] It was demonstrated in previous studies that the PBE-TS functional accurately reproduces crystal structure data of neutral-framework zeotypes,[41,42] and good agreement with experimental vibrational spectra was observed in investigations of a hydrated aluminophosphate[43] and of two titanium pyrophosphates.[44] The calculations used a plane-wave cutoff energy of 700 eV and on-the-fly ultrasoft pseudopotentials. Due to the presence of V^{4+} cations, spin-polarized calculations were carried out for all systems under study: On the one hand, two fully ordered models of VSH-2Cs (space groups $Cmc2_1$ and *Cm2a*, see 2.2) were compared, optimizing all atomic coordinates, but fixing the cell parameters to experimental values. The calculations used a 2×2×2 mesh of *k*-points to sample the first Brillouin zone.

The DFT energy difference between the two optimized structures was very small, amounting to 7.7 meV (−0.74 kJ mol^{-1}) per formula unit. This indicates that there is no strong energetic preference for either of the fully ordered arrangements, in line with the experimental observations. After the structure optimizations, phonon calculations using the finite displacement method[45] were performed to compute the frequencies of IR active modes. These calculations were carried out on a supercell having twice the size of the conventional cell of VSH-2Cs. All reported frequencies were scaled by a factor of 0.985, which has been proposed previously for use with the PBE functional.[46] The transferability of the scaling factor to CASTEP plane-wave calculations was verified through a calculation of the O–H stretching frequencies of an isolated water molecule (CASTEP, scaled: 3648 cm^{-1}, 3754 cm^{-1}, experiment: 3657 cm^{-1}, 3756 cm^{-1}).

For VSH-2Li, two different models were generated, removing the disorder from the crystal structure: Model *a* represents the case in which the Li^+ ions fully occupy the extraframework positions, while the model *b* corresponds to an alkali deficient framework in which H_3O^+ ions balance the framework charge. For model *a*, all atomic positions were fully relaxed and a phonon calculation was performed, using essentially analogous settings to those described above for VSH-2Cs. For model *b*, however, a full structure relaxation inevitably resulted in a transfer of the protons from the hydronium ions to the V=O group, in disagreement with experimental observations. Therefore, only the H atom positions were relaxed in this structure, and all other atoms were fixed at their experimental positions.

Acknowledgements

We thank Stefan Heissler for collecting the ATR-FTIR data and Kirsten Drüppel for collecting the SEM images and EDX spectra. MF acknowledges funding by the German Research Foundation (Deutsche Forschungsgemeinschaft – DFG) through a Heisenberg grant (grant no. 455871835). Three anonymous reviewers are acknowledged for the constructive comments. Open Access funding enabled and organized by Projekt DEAL.

Conflict of Interests

The authors declare no conflict of interest.

Data Availability Statement

The data that support the findings of this study are available from the corresponding author upon reasonable request.

Keywords: zeotype materials · lithium ion-exchange · phase transformation · protonated water clusters · materials chemistry

[1] L. Nemeth, S. R. Bare, *Adv. Catal.* Vol. 57 (Ed.: F. C. Jentoft), Academic Press, **2014**, pp. 1–97.
[2] J. S. Meshram, D. S. Raghuvanshi, *Curr. Green Chem.* **2021**, *8*, 17–27.
[3] E. T. C. Vogt, G. T. Whiting, A. Dutta Chowdhury, B. M. Weckhuysen, *Adv. Catal.*, Vol. 58 (Ed.: F. C. Jentoft), Academic Press, **2015**, pp. 143–314.
[4] C. Freire, C. Pereira, B. Jarrais, D. Fernandes, A. Peixoto, N. Cordeiro, F. Teixeira, *RSC Catal.*, Chapter 11: Supported Vanadium Catalysts: Heterogeneous Molecular Complexes, Electrocatalysis and Biomass Transformation, **2021**, vol. 2021 - Januar.
[5] I. E. Wachs, *Dalton Trans.* **2013**, *42*, 11762–11769.
[6] M. Wark, A. Brückner, T. Liese, W. Grünert, *J. Catal.* **1998**, *175*, 48–61.
[7] P. Brandão, A. Philippou, N. Hanif, P. Ribeiro-Claro, A. Ferreira, M. W. Anderson, J. Rocha, *Chem. Mater.* **2002**, *14*, 1053–1057.
[8] P. Brandão, A. Valente, A. Philippou, A. Ferreira, M. W. Anderson, J. Rocha, *Eur. J. Inorg. Chem.* **2003**, 1175–1180.
[9] R. M. Barrer, J. Klinowski, *J. Chem. Soc. Faraday Trans. 1* **1972**, *68*, 1956–1963.
[10] G. M. Johnson, B. A. Reisner, A. Tripathi, D. R. Corbin, B. H. Toby, J. B. Parise, *Chem. Mater.* **1999**, *11*, 2780–2787.
[11] N. Döbelin, T. Armbruster, *Microporous Mesoporous Mater.* **2007**, *99*, 279–287.
[12] V. M. Georgieva, E. L. Bruce, R. G. Chitac, M. M. Lozinska, A. M. Hall, C. A. Murray, R. I. Smith, A. Turrina, P. A. Wright, *Chem. Mater.* **2021**, *33*, 1157–1173.
[13] G. M. Johnson, B. A. Reisner, A. Tripathi, D. R. Corbin, B. H. Toby, J. B. Parise, *Chem. Mater.* **1999**, *11*, 2780–2787.
[14] X. Wang, L. Liu, A. J. Jacobson, *Angew. Chem. Int. Ed.* **2001**, *79*, 2174–2176.
[15] X. Wang, L. Liu, A. J. Jacobson, *J. Am. Chem. Soc.* **2002**, *124*, 7812–7820.
[16] R. M. Danisi, F. R. Schilling, *Microporous Mesoporous Mater.* **2021**, *319*, 111064.
[17] S. J. Datta, K. B. Yoon, *Top. Catal.* **2010**, *53*, 1311–1318.
[18] S. J. Datta, K. B. Yoon, *Angew. Chem. Int. Ed.* **2010**, *49*, 4971–4975.
[19] S. J. Datta, K. B. Yoon, *Microporous Mesoporous Mater.* **2011**, *143*, 115–124.
[20] B. Liu, R. Zhang, C. Y. Pan, H. L. Jiang, *Inorg. Chem.* **2017**, *56*, 4263–4266.
[21] M. I. Aroyo, J. M. Perez-Mato, D. Orobengoa, E. Tasci, G. De La Flor, A. Kirov, *Bulg. Chem. Commun.* **2011**, *43*, 183–197.
[22] G. Bergerhoff, M. Berndt, K. Brandenburg, T. Degen, *Acta Crystallogr. Sect. B* **1999**, *55*, 147–156.
[23] M. Wenger, T. Armbruster, *Eur. J. Mineral.* **1991**, *3*, 387–400.
[24] D. Orobengoa, C. Capillas, M. I. Aroyo, J. M. Perez-Mato, *J. Appl. Crystallogr.* **2009**, *42*, 820–833.
[25] E. Libowitzky, *Hydrogen Bond Res.* **1999**, *1059*, 103–115.
[26] D. E. Resasco, S. P. Crossley, B. Wang, J. L. White, *Catal. Rev. Sci. Eng.* **2021**, *63*, 302–362.
[27] I. D. Brown, *Acta Crystallogr. Sect. A* **1976**, *32*, 24–31.
[28] O. Markovitch, H. Chen, S. Izvekov, F. Paesani, G. A. Voth, N. Agmon, *J. Phys. Chem. B* **2008**, *112*, 9456–9466.
[29] O. Ferro, S. Quartieri, G. Vezzalini, C. Ceriani, E. Fois, A. Gamba, G. Cruciani, *Am. Mineral.* **2004**, *89*, 94–101.
[30] A. Alberti, A. Martucci, *J. Phys. Chem. C* **2010**, *114*, 7767–7773.
[31] G. M. Sheldrick, *Acta Crystallogr. Sect. C* **2015**, *71*, 3–8.
[32] A. L. Spek, *J. Appl. Crystallogr.* **2003**, *36*, 7–13.
[33] T. Bauer, W. H. Baur, *Eur. J. Mineral.* **1998**, *10*, 133–147.
[34] K. Momma, F. Izumi, *J. Appl. Crystallogr.* **2011**, *44*, 1272–1276.
[35] R. Hoppe, *Z. Kristallogr.* **1979**, *150*, 23–52.
[36] I. D. Brown, D. Altermatt, *Acta Cryst.* **1985**, *244*, 244–247.
[37] M. Nespolo, *J. Appl. Cryst.* **2016**, 317–321.
[38] S. J. Clark, M. D. Segall, C. J. Pickard, P. J. Hasnip, M. I. J. Probert, K. Refson, M. C. Payne, *Z. Kristallogr.* **2005**, *220*, 567–570.
[39] J. P. Perdew, K. Burke, M. Ernzerhof, *Phys. Rev. Lett.* **1996**, *77*, 3865–3868.
[40] A. Tkatchenko, M. Scheffler, *Phys. Rev. Lett.* **2009**, *102*, 073005.
[41] M. Fischer, F. O. Evers, F. Formalik, A. Olejniczak, *Theor. Chem. Acc.* **2016**, *135*, 257.
[42] M. Fischer, W. J. Kim, M. Badawi, S. Lebègue, *J. Chem. Phys.* **2019**, *150*, 094102.
[43] M. Fischer, Molecules DOI: 10.3390/molecules24050922.
[44] H. Petersen, N. Stegmann, M. Fischer, B. Zibrowius, I. Radev, W. Philippi, W. Schmidt, C. Weidenthaler, *Inorg. Chem.* **2022**, *61*, 2379–2390.
[45] W. Frank, C. Elsässer, M. Fähnle, *Phys. Rev. Lett.* **1995**, *74*, 1791–1794.
[46] I. M. Alecu, J. Zheng, Y. Zhao, D. G. Truhlar, *J. Chem. Theory Comput.* **2010**, *6*, 2872–2887.
[47] Bruker, SADABS, Bruker AXS Inc., Madison, Wisconsin, USA, **2003**.

Manuscript received: June 3, 2023
Revised manuscript received: August 9, 2023
Accepted manuscript online: August 16, 2023
Version of record online: ■■, ■■

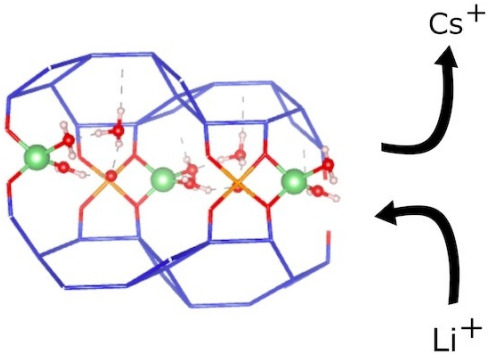

Dr. R. M. Danisi, Dr. M. Fischer**

Cooperative rotation of SiO_4 and VO_5 units in response to Li-ion exchange led to changes in symmetry in VSH-2 framework. The Cs sites are converted into new distorted tetrahedral sites for smaller Li^+ ions via 2D ion transport along the [011] direction. Exchange of Cs^+ by Li^+ is incomplete suggesting the formation of protonated water clusters to counterbalance the net negative framework charge.